

Evolution of galaxy overdensities around 3C radio galaxies and quasars at $1 < z < 2.5$ revealed by *Hubble* 0.6/1.4 μm and *Spitzer* 3.6/4.5 μm

Z. Ghaffari^{1,*}, M. Haas¹, M. Chiaberge², S. P. Willner³, M. L. N. Ashby³, B. J. Wilkes³, R. Chini^{1,4}, M. West⁵, and R. de Propris⁶

¹ Astronomisches Institut, Ruhr-Universität Bochum, Universitätsstraße 150, 44801 Bochum, Germany

² Space Telescope Science Institute, 3700 San Martin Drive, Baltimore, MD 21218, USA

³ Harvard-Smithsonian Center for Astrophysics, 60 Garden St., Cambridge, MA 02138, USA

⁴ Instituto de Astronomía, Universidad Católica del Norte, Avenida Angamos 0610, Casilla 1280 Antofagasta, Chile

⁵ Lowell Observatory, 1400 West Mars Hill Road, Flagstaff, AZ 86001, USA

⁶ Finnish Centre for Astronomy with the European Southern Observatory, University of Turku, Väisäläntie 20, 21500 Piikkiö, Finland

Received XXXX, accepted XXXX

Published online XXXX

Key words high-redshift — clusters of galaxies

A random sample of 21 high-redshift 3C sources at $1 < z < 2.5$ has been mapped with the *Hubble Space Telescope* (~ 28 and 25 AB mag at 0.6 and 1.4 μm , resp.) and the *Spitzer Space Telescope* (22.4 AB mag at 3.6 and 4.5 μm). In about 130'' field of view, essentially all *Spitzer* detected sources are also detected with *Hubble*. In addition, the images show faint *Hubble* detected sources with only upper limits at 3.6 and 4.5 μm . We apply two methods to select candidate cluster member galaxies. 1) Template fitting of the spectral energy distributions and color selection allows us to reject foreground sources and to identify the brightest candidate cluster member galaxies at the redshift of the radio source. 2) We simply select candidates via a brightness cut $22 \text{ mag} < F140W < 24 \text{ mag}$. Both methods yield consistent results. About half of the 3C radio sources show significant overdensities ($> 3\sigma$) within 30'' (~ 250 kpc) projected distance from the radio source compared to the surrounding galaxy densities measured in the 30''–70'' annulus. Compared to higher redshifts, at $z < 1.4$ the overdensities are, on average, more pronounced and essentially caused by red galaxies, while blue galaxies show a trend of avoiding the cluster center, i.e. a central underdensity. On the other hand, at $z > 1.5$ we find increasing overdensities made up of blue galaxies. We interpret the results as evolution of overdensities from being composed of mainly blue (starforming) galaxies at $z = 2.5$ to mainly red (presumably elliptical) galaxies at $z = 1$.

Copyright line will be provided by the publisher

1 Introduction

Clusters of galaxies belong to the largest structures in the universe. To find them at high redshift ($z > 1$) proved difficult. Searching for the signatures of the hot intracluster medium (ICM) and the SZ effect, X-ray and millimeter observations found clusters up to $z \sim 1.5$ (TBD: some references). An open issue is whether at $z > 1.5$ already sufficient ICM has assembled. Wide field optical and near-infrared (NIR) surveys likewise identified a growing number of overdensities of cluster members (or candidates) up to $z \sim 1.5$ with a few proto-clusters reaching $z \sim 3$ (TBD: some references).

High-redshift radio galaxies (HzRGs) belong to the most massive host galaxies in the universe (e.g., Seymour et al. (2007) and references therein) and are consequently suspected to reside in galaxy proto-clusters or clusters (Miley & De Breuck 2008). Several studies on high redshift 3Cs (Best 2000; Best et al. 2003) and other radio galaxy samples (Galametz et al. 2012; Venemans et al. 2007; Wylezalek

et al. 2013) revealed an average overdensity of galaxies around the radio source up to $z \sim 3$.

The high redshift 3C sample consists of 64 radio galaxies and quasars at $1 < z < 2.5$ (Spinrad et al. 1985). They all have been observed with *Spitzer/IRAC* (3.6 – 8 μm) and MIPS (24 μm) with a nearly 100% detection rate (Haas et al. 2008). A random sub-sample of 22 high-z 3Cs has been observed with the *Hubble Space Telescope* (*HST*) in the *F606W* (606 nm) and *F140W* (1.4 μm) filters (Hilbert et al. 2016). The 3C's environment has been studied by Ghaffari et al. (2017) using the *Spitzer IRAC1/2* 3.6 and 4.5 μm images in combination with the *PanStarrs (PSO)* *i* band images, and by Kotyla et al. (2016) using the *HST* images. For a more detailed introduction the reader is referred to Kotyla et al. (2016) and Ghaffari et al. (2017).

In brief, recalling the results and open issues from Ghaffari et al. (2017) on the *Spitzer – PSO* study:

- two color criteria, using *IRAC1/2* and *IRAC-PSO*, to reject foreground sources,
- both criteria yield, on average, 50% overdensities (ODs) within 30'' (250 kpc) projected radius,

* Corresponding author: ghaffari@astro.rub.de

Copyright line will be provided by the publisher

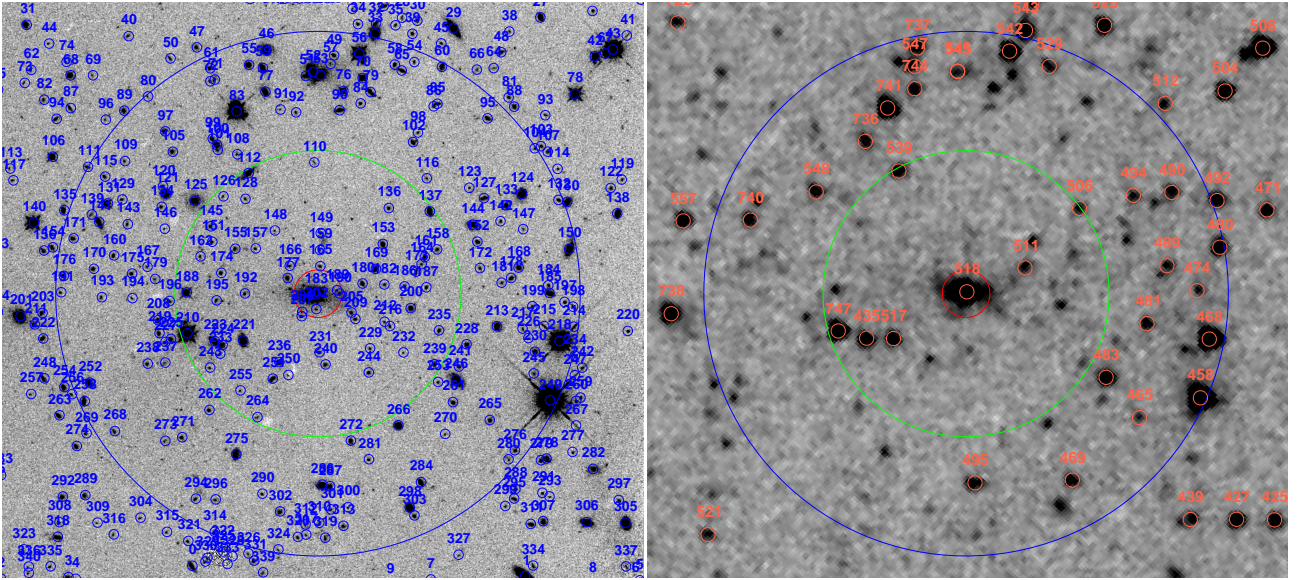


Fig. 1 Images of the quasar 3C 186 with *HST F140W* (left) and *Spitzer IRAC1* (right). The red circles of 5'' radius mark the 3C source. The large circles (green/blue) have a radius of 30'' and 55'', respectively. The small blue and red circles mark each catalogue galaxy for *HST* (blue, 1.0'') and *IRAC* (red, 1.5''), labeled with its catalog identification number. North is towards the upper left corner.

- in addition, the *IRAC-PSO* cut reveals a redshift trend: decline of ODs beyond $z = 1.4$,
- for a stronger *IRAC1/2* color cut the ODs at $z < 1.4$ disappear; because this color cut removes preferentially elliptical galaxies, the ODs found with the softer color cut likely consist of ellipticals.

Open issues: 1) The color cuts may have rejected only a limited number of foreground sources, because of the PSO upper limits ($i < 21.75$ mag). 2) Most of the blue sources may have escaped the detection by *IRAC*. Therefore, deep optical imaging would be desired.

Recalling the results and open issues from Kotyla et al. (2016) on the *HST* study:

- identification of red sequences of those galaxies with early type morphology (Sersic Index $2 < n < 8$),
- identification of overdensities using all galaxies within 40'' radius around the 3Cs, compared to GOODs fields,
- both methods yield, on average, 50% overdensities around the 3Cs,
- discovery of a “blue sequence” for 3C 257 at $z = 2.47$, the highest redshift 3C source.

Open issues: 1) For faint sources ($F140W > 22$ mag) the determination of the Sersic Index becomes uncertain. The narrow color range for red sequences assumes passive evolution, although galaxy interactions are expected to occur during the cluster assembly. 2) Because GOODs fields are at high galactic latitude, the comparison with 3Cs at lower latitude may be biased; therefore it would be desirable to check for a radial density decline within the *HST* fields.

For studying the evolution of ODs in the early universe with as little biases as possible, the environment of HzRGs appears particularly attractive. These mass signposts are homeogeneously selected by their FR II radio lobes.

Here, we present a *Spitzer – HST* study of the environment of 21 high- z 3Cs, 9 quasars and 12 radio galaxies. As in Kotyla et al. (2016), we removed 3C 418, because it lies close to the galactic plane and is strongly contaminated by stars. Given the 30'' projected radius for ODs found by the *Spitzer-PSO* study, the *HST* Field-of-View (130'') should be large enough to identify a radial density decline. A particular advantage is the high detection rate: 99% of the *IRAC* 3.6 and 4.5 μm sources are now also detected at optical-NIR wavelengths (0.6 and 1.4 μm). Less than 2% of the *IRAC* sources have multiple matches.

This paper is organized as follows. Section 2 describes the data, including the matched *Spitzer – HST* source catalog and the correction for the foreground galactic extinction. Section 3 shows example SEDs. Section 4 briefly comments on the Sersic Index. Section 5 describes the method 1 to select candidate cluster member galaxies. Section 6 reports on the ODs. Section 7 discusses the results and issues and compares with an alternative method 2 of candidate selection. A summary is presented in Section 8. Throughout this work we adopt a standard ΛCDM cosmology ($H_0 = 70 \text{ km s}^{-1} \text{ Mpc}^{-1}$, $\Omega_\Lambda = 0.73$, and $\Omega_m = 0.27$ (Spergel et al. 2007). All magnitudes are AB where zero mag corresponds to 3631 Jy.

2 Data

The sample is listed in Table 1. Figure 1 shows images of an example, the quasar 3C 186.

2.1 *Spitzer / IRAC*

The sample was mapped with *Spitzer* using *IRAC* (and *MIPS* 24 μm). The *IRAC* FoV is about 4.5 arcmin. The

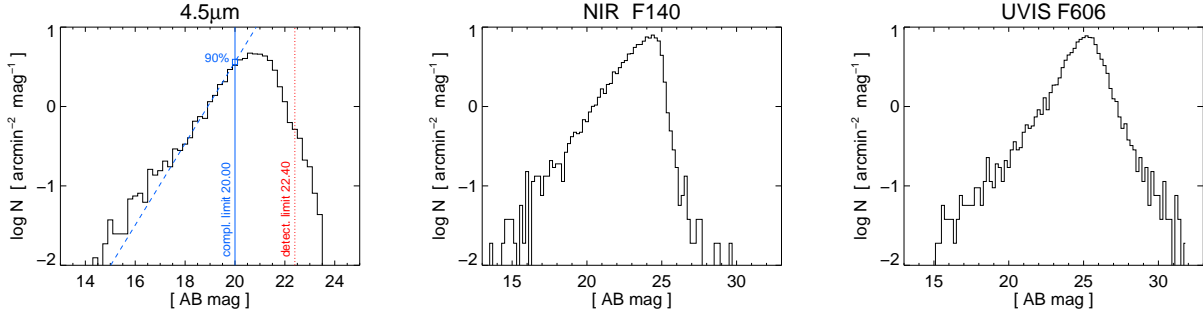


Fig. 2 Log(N) versus magnitude histograms of the entire sample. The detection limit (the magnitude at which 98% of the sources are brighter) reaches 25.5 mag for $F140W$ and 29 mag for $F606W$. However, the completeness limits ($\sim 90\%$) are 24.5 AB mag for both filters, the HST source catalog contains only those $F606W$ sources which are also detected in $F140W$.

source catalog was created using the *IRAC* 2 ($4.5 \mu\text{m}$) images as primary catalog. To better exclude false detections, all sources had also to be detected with *IRAC* 1 ($3.6 \mu\text{m}$). For both filters the detection and 90% completeness limits are about 22.4 mag and 20 mag, respectively. In the following we reject sources brighter than 16 mag and more extended than $4''$ Kron radius, because they are likely foreground sources. For more details see Ghaffari et al. (2017).

2.2 *HST*

The sample was mapped with HST using WFC3 in the filters $F606W$ and $F140W$ (Hilbert et al. 2016). The source catalog was created using the $F140W$ as primary catalog, whereby all sources had also to be detected with $F606W$ (Kotyla et al. 2016). The image sizes are $124'' \times 136''$. Accounting for a small border, the area is 4.3 square arcmin. For more details we refer the reader to Kotyla et al. (2016).

2.3 Cross-matched *HST* and *Spitzer* catalog

All source photometry is corrected for foreground galactic extinction (Schlafly & Finkbeiner 2011).

We cut the *Spitzer* catalog to the FoV of the HST images. We corrected for a small systematic positional offsets between *IRAC* and HST sources. Therefore, for each 3C field, we performed two iterations of the matching: in the first iteration we determined the median offset between *IRAC* and HST using a matching radius of $1''.5$. The median offset is about $0''.5$. In the second iteration, we matched the offset-corrected positions using a matching radius of $1''.0$.

About 99% of the *IRAC* sources are matched with an HST source. Only about 2% of the *IRAC* sources have a multiple HST match; they are removed from the matched HST and *Spitzer* catalog.

The matched HST and *Spitzer* catalog of the 21 3C sources contains 1394 $HST + IRAC$ sources and 3522 HST only sources.

3 SED examples

Figure 3 shows SED of four typical sources in the field of 3C 186 along with four local galaxy SED templates. The templates are NGC 6946 blue SF spiral galaxy; Arp 220 is an ultraluminous infrared galaxy (ULIRG); NGC 221 is an old elliptical and (NGC 2146) is a reddened SF galaxy.

Figure 4 illustrates the disentangling of close sources. Figure 5 shows an example of an HST only source which is very faint on the *Spitzer* images, and therefore has only an *IRAC* $3-\sigma$ upper limit.

4 Sersic Index

For each $HST F140W$ source we performed a new determination of the Sersic Index N independent of that by Kotyla et al. (2016), using the GALFIT package (Peng et al. 2010). For sources brighter than $F140W = 22$ mag the Sersic Index results appear reliable as illustrated by Figure 3: for the source which is best fitted by a blue SF galaxy GALFIT yields $N = 0.87$, consistent with expected $N = 1$. The two sources best fitted by a red template yield N between 2.5 and 3.4, again consistent with expectations for early type galaxies and morphologically disturbed galaxies. Nevertheless, as already discussed by Kotyla et al. (2016), the Sersic Index classification becomes uncertain for fainter sources ($F140W > 22$ mag), simply because they usually have not enough pixels with sufficient S/N.

5 Selection of candidate galaxies (Method 1)

We identify the candidate cluster member galaxies at the redshift of the 3C targets by two criteria: If the source is detected with HST and *Spitzer* we apply a quasi static SED fitting. If the source is only detected by HST we apply a color cut.

5.1 *Spitzer* and HST detections

For sources detected with HST and *Spitzer*, we use the four photometry data points at 0.6, 1.4, 3.6 and $4.5 \mu\text{m}$. The

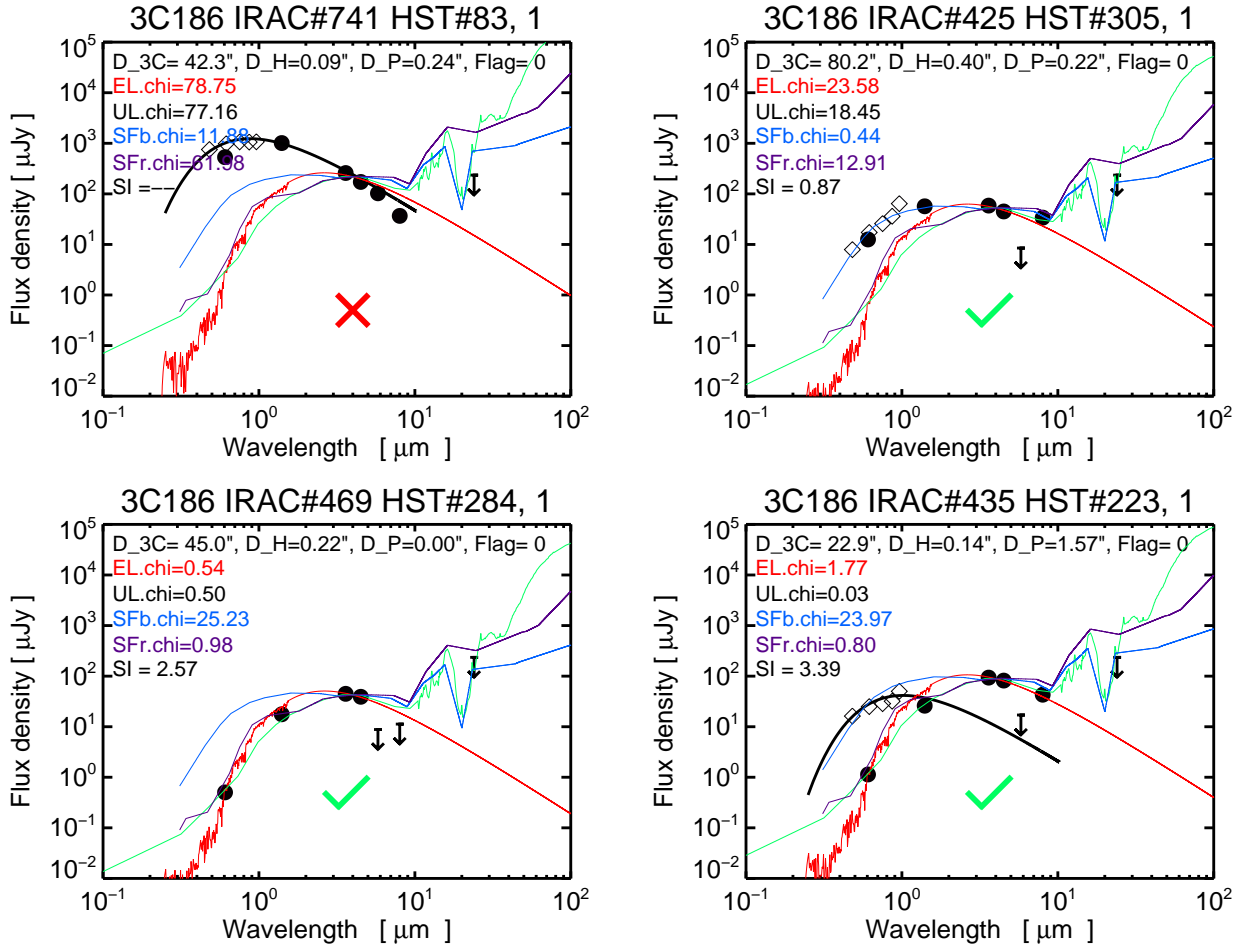


Fig. 3 Four example SEDs of galaxies in the field of 3C 186. The SEDs shown are typical for all sources which are detected with both *HST* and *Spitzer*. Black dots are *HST* and *Spitzer* data, black arrows denote 3- σ upper limits, error bars are smaller than the symbol size. Diamonds are *Pan-Starrs* (*PSO*) data. The distance of the *IRAC* source from 3C 186, the next *HST* source and the next *PSO* source are given (D_3C, D_H and D_P, respectively). Flag = 0 means good photometric quality. The four colored solid lines depict local galaxy templates shifted to the redshift $z = 1.069$ of 3C 186: red = elliptical galaxy (NGC 221), green = ultraluminous infrared galaxy (ULIRG, Arp 220), blue = blue star forming spiral galaxy (NGC 6946), purple = red star forming spiral galaxy (NGC 2146). The reduced chi square values of each template are as labeled. SI gives the Sersic Index N. The check mark (green) and cross (red) show accepted (chi square < 1.5) and rejected candidates. **Top-left:** Foreground source, much brighter in *HST* and *PSO* than *Spitzer*-*IRAC*. The solid black line shows a Planckian fit through the *PSO* and *IRAC* 1+2 data. **Top-right:** The data agree with a blue star forming galaxy at the 3C's redshift. **Bottom-left:** The data agree with an Elliptical, ULIRG and red star forming galaxy. **Bottom-right:** The data agree best with a ULIRG and a red star forming galaxy and – if allowing for larger chi square tolerance – also with an Elliptical. The nearby *PSO* source is well separated by 1''.57 as shown in Fig. 4. The solid black line shows a Planckian fit through the *PSO* data and its F140W flux (not plotted to avoid confusion).

IRAC 3/4 (and *MIPS*) data points are not used here, because they are often uncertain upper limits.

With the limited set of four photometry data points any arbitrary SED fitting will be coarse and unreliable. Therefore, we here tried the following quasi static SED fitting:

We used four local templates as described above, shifted them to the redshift of the 3C source (“quasi static”). Then for each object we fitted the redshifted template to the source’s SED, i.e. adjusted the template brightness and calculated the reduced chi square. An object is accepted as candidate, if at least one of the templates yields a reduced chi square of less than 1.5. This is illustrated in Figure 3.

In principle, this SED fitting technique is equivalent to a multi-color selection, whereby the color ranges are derived from the redshifted templates. The major advantage of the SED fitting technique is its simplicity. We discuss the influence of choosing local templates further below (Sect. 7).

5.2 *HST* only detections with *Spitzer* upper limits

For *HST* only sources we selected candidate cluster member galaxies as follows: We shifted each of the four templates to the redshift of the 3C source, determined the template F606W – F140W color and a color tolerance range ± 0.3

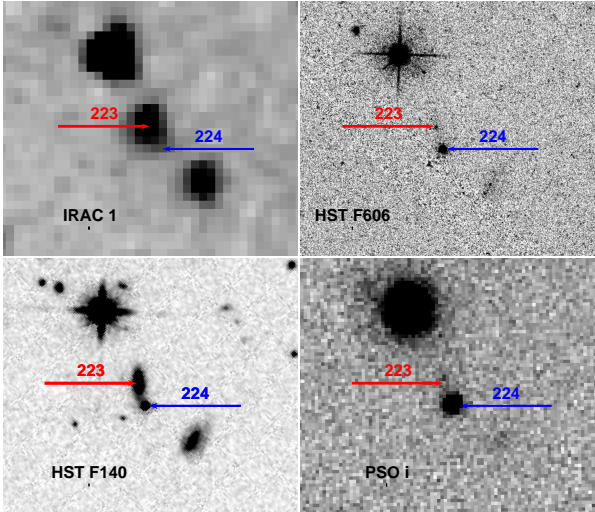


Fig. 4 Example of disentangling close sources in the field of 3C 186. The *HST* sources id-223 and id-224 are separated by $1''57$. The elliptical galaxy id-223 (marked by the red arrow) coincides with the *IRAC 1* source (IRAC id-435 in Fig. 3, bottom right), while the point source id-224 (marked by the blue arrow) coincides with a *PanStarrs i* band source not detected with *IRAC*.

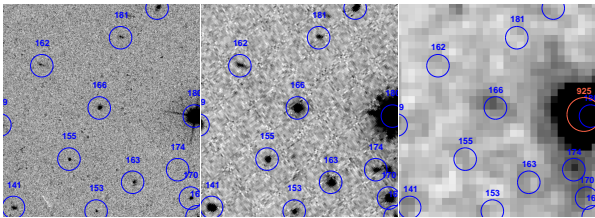


Fig. 5 Images centered on a faint object in the field of 3C 432 at $z = 1.785$. **Left:** *HST* $0.6\mu\text{m}$, **middle:** *HST* $1.4\mu\text{m}$, **right:** *Spitzer* $3.6\mu\text{m}$. The faint source in the image centre is not contained in the *IRAC* catalog and treated as an upper limit for *Spitzer*. The blue and red circles have $1''.0$ and $1''.5$ radius. They are labeled with *HST* id and *IRAC* id, respectively.

mag. Then a source is accepted as candidate, if its color falls into the color range of at least one of the four redshifted templates.

5.3 Summary of candidate selection

The number of candidates of galaxies found at the redshift of the 3C source are:

All candidates: 1591

HST + IRAC matched: 419

HST only: 1172

The templates ULIRG and SFr are a bit bluer than the Elliptical template. As discussed in Section 7, at high redshift the Ellipticals might be bluer than our template. In the following we consider only two types of galaxies: red (ULIRG, SFr, Ell.) and blue (SFb).

HST red: 165

HST blue: 1007

The fraction of candidates/all galaxies is similar for the *HST + IRAC* and the *HST only* subsamples:

HST + IRAC: $419 / 1394 = 30\%$, i.e. 70% foreground+background

HST only: $1172 / 3522 = 33\%$, i.e. 68% foreground+background

Thus, we do not expect any bias by combining the candidate samples *HST + IRAC* and *HSTonly*.

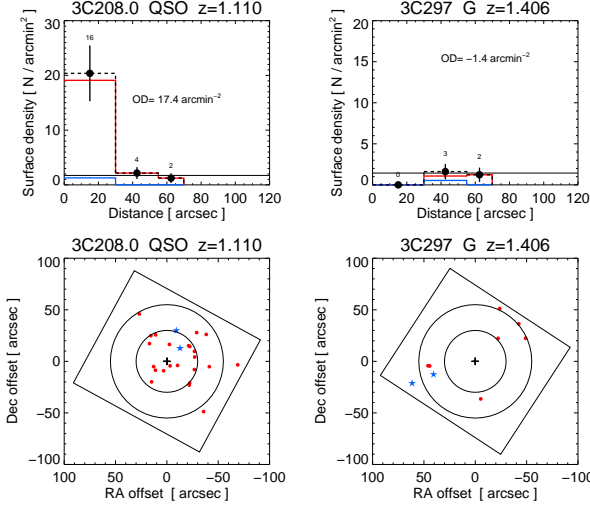


Fig. 6 *HST+IRAC* detected sources: **Top:** Radial surface density of candidate cluster member galaxies for two examples, 3C 208.0 and 3C 297 with and without a clear central overdensity. The candidate cluster member galaxies were selected with a quasi static template SED fitting method. The red and blue solid lines show the distribution of red and blue candidates, respectively. The black dashed line shows the distribution of all candidates. Numbers show the number of candidates in each radial bin. Error bars show Poisson uncertainty in each bin. The horizontal black solid line marks the average density determined from the two outer annuli at $30'' - 70''$. The excess density as labeled gives the density inside $30''$ above the mean surrounding density. The 3C source is not counted in the radial density plots. The examples are typical for the entire sample. **Bottom:** Schematic map of the candidates. The filled red circles are red galaxy candidates and the blue filled stars are blue galaxy candidates. The black “+” marks the position of the 3C source. For 3C 208.0 the overdensity is clearly dominated by red sources.

6 Galaxy overdensities

To check for galaxy overdensities, we defined three radial bins: the central bin with radius $30''$ and two rings ($30'' - 55''$) and $> 55''$ (which is effectively similar to $55'' - 70''$). We counted the number of selected candidates in each bin. The 3C source itself is excluded from the counts.

6.1 Radial surface density profiles

Fig. 6 and Fig. 7 show examples of radial density profiles of the selected candidate galaxies at the 3C’s redshift as well as schematic sky maps. The striking features of these two Figures are:

- *HST+IRAC* detected sources (Fig. 6):
 - some 3Cs show overdensities and some do not,
 - most 3Cs with clear OD are at “low” redshift $1 < z < 1.5$,
 - overdensities, if found, are mostly made up of red galaxies.
- *HST+IRAC* detected and *HST only* sources (Fig. 7):
 - the number of candidates is considerably larger,

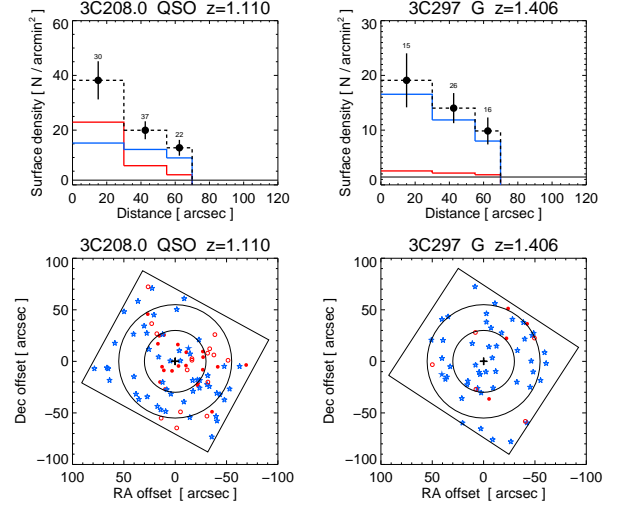


Fig. 7 Same as Fig. 6 but for all sources, i.e. *HST+IRAC* detected and *HST only* sources. **Top:** Radial surface density of candidate cluster member galaxies. **Bottom:** The filled symbols mark the *HST+IRAC* detected sources. Open symbols (red circles & blue stars) mark the *HST “Only”* selected candidates.

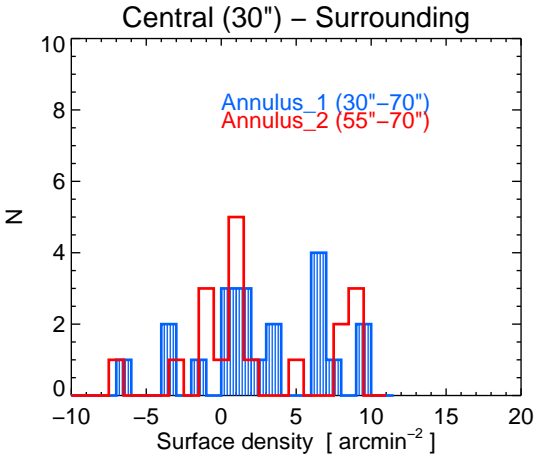


Fig. 8 Distribution of the central overdensities, that is, central surface density minus surrounding surface density (Annulus 1 and 2, respectively). For both annuli the distributions are similar and show a large spread.

- some 3Cs show overdensities and some do not,
- the inclusion of the *HST* only candidates typically reveals an OD of blue galaxies in those 3Cs with no OD in the *HST+IRAC* detected sample,
- the inclusion of the *HST* only candidates typically reveals an OD of red galaxies in those 3Cs with OD in the *HST+IRAC* detected sample,
- most 3Cs with clear OD are at “low” redshift $1 < z < 1.5$.

6.2 Statistics of the overdensities

Fig. 8 shows the histogram of the central overdensities, computed with all candidates (*HST+IRAC* and *HST only*).

The distribution shows a broad dispersion. Table 1 lists all numbers regarding the overdensities.

A better statistical information can be retrieved from cumulative distributions, in particular, *after sorting the 3C sources by redshift*.

Fig. 9 shows the cumulative surface densities for all three radial bins, separated for all sources, for the blue sources and the red sources. In total the central surface densities lie above the densities of the two outer annuli. These annuli show similar cumulative surface densities.

Fig. 10 shows the cumulative overdensities. The overdensities are the central surface densities after subtraction of the outer annulus ($> 55''$).

A striking feature of the diagrams in Fig. 10 is:

- For all sources (left panel), the cumulative overdensities on average follow a linear trend, embraced by the blue and red parallel lines. There is a remarkable change in slope at about $z = 1.4$.
- For the red sources (middle panel), the cumulative overdensities on average show a strong gradient change at about $z = 1.24$. They steeply rise until $z < 1.24$ and remain roughly constant at higher redshift. Compared with the left panel (c.f. the two parallel lines), we can conclude that at “low” redshift ($1 < z < 1.4$) the OD is essentially built up by red candidates, and at “high” redshift the OD is dominated by blue candidates.
- For the blue sources (right panel), the cumulative overdensities on average remain constant (or even decline slightly) until $z \sim 1.24$, then steeply rise until $z \sim 1.6$ and remain roughly constant at higher redshift.

7 Discussion

The results in Fig. 10 show a remarkable evolution of the ODs from being composed of mainly red (presumably elliptical) galaxies at $z = 1$ to mainly blue (starforming) galaxies at $z > 1.5$. However, the results depend on the choice of the local template galaxies and their colors. So far, we did not take into account galaxy evolution and that galaxies at high redshift are “younger” and may have bluer colors. This effect may be negligible for the blue SF template but likely becomes more relevant for the Elliptical template, which at high redshift might have bluer colors, perhaps like those of the ULIRG and the red SF template. Notably, many if not most of the red candidates were selected due to resembling the colors of the ULIRG and the red SF template. This would alleviate the concerns a bit. For further comparison, we denote the selection of the candidates via template fitting and color ranges “selection method 1”.

For comparison, the red sequence color ranges used by Kotyla et al. (2016, their Figs. 2 and 3) strongly depend on the redshift. They are similar to ours used here for $z < 1.4$ but become bluer for higher redshift. Kotyla et al. use GalEv (Kotulla et al. 2009), the evolutionary synthesis modeling

program. The GalEv input parameters include mass, metallicity, and redshift of formation. For their models, they assume a single burst of star formation followed by passive evolution, using two galaxy formation redshifts $z = 6.5$ and $z = 20$. From simulations, however, one would expect that during the cluster assembly many galaxy interactions and mergers occur, as shown in Figure 5 of West (1994), questioning the assumption of passive evolution.

In order to check the ODs independent of any template choices and of assumptions on the evolution of galaxies and their colors, we performed the following candidate selection experiment, henceforth called “selection method 2”:

In Appendix A we show CMDs for several 3C fields (Figs. 14 - 20, sorted by increasing redshift). Each Figure shows six panels, each for a specific area (i.e. annulus). First we separate the samples by the color threshold $F606W - F140W = 2.0$ (horizontal long-dashed lines). This yields red and blue candidates (marked by red circles and blue asterisks). Based on the experience with the SEDs, we make the reasonable assumption that bright sources ($F140W < 22$ mag) are essentially foreground sources. Furthermore, for very faint sources ($F140W > 24$ mag) there appears a deficit of red sources ($F606W - F140W > 2.0$); its origin is not yet clear (see Appendix B). Therefore, in order to avoid color biases as far as possible, we select only sources in the brightness range $22 < F140W < 24$.

Then we performed the same OD analysis on these sources, as we did for method 1, calculating the radial surface density in the three radial bins. The resulting cumulative overdensities are shown in Fig. 11, for all sources and the red and blue sources. The striking features of the cumulative overdensities are:

- all sources: the cumulative overdensities, on average, rise between $z = 1$ and $z = 1.4$ and flatten (or even turn over) at higher redshift,
- red sources: the cumulative overdensities rise and turn over at $z \sim 1.8$,
- blue sources: the cumulative overdensities slightly decline and become constant at $z \sim 1.6$.

The results for selection method 2 (Fig. 11) yield smaller overdensities as measured in total numbers, but they are remarkably consistent with those found from selecting the candidates via method 1, i.e. fitting color ranges of local templates (Fig. 10).

The smaller absolute overdensity numbers for method 2 (compared to method 1) could indicate that the clusters are “extended” within the relatively small FoV, i.e. show many cluster member galaxies out to $70''$ radius. Note that $70''$ radius corresponds to about 583 kpc projected radius (for all redshifts of our sample).

The overdensity decline of the blue sources can be interpreted as a central underdensity. This means that blue sources are preferentially in the outskirts of the forming clusters. To corroborate this suggestion and to check whether the surface density of blue galaxies declines further out, larger images would be required; we have already

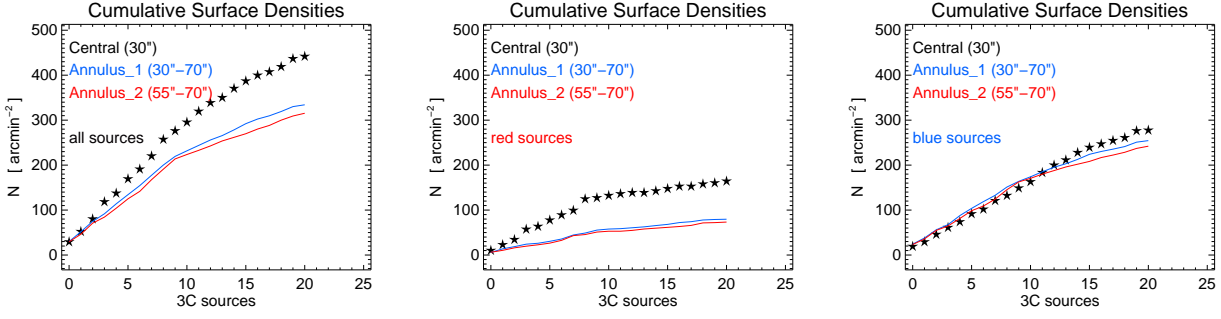


Fig. 9 Cumulative surface densities using method 1. Left: all candidates, middle: red candidates, right: blue candidates. Black asterisks mark the central bin, the solid blue and red lines mark the annuli. The X-axis refers to the index of the 3C sources sorted by redshift, i.e., $z \approx 1.0$ at $X=1$, $z \approx 1.4$ at $X=11$, $z \approx 1.7$ at $X=17$, and $z \approx 2.5$ at $X=21$.

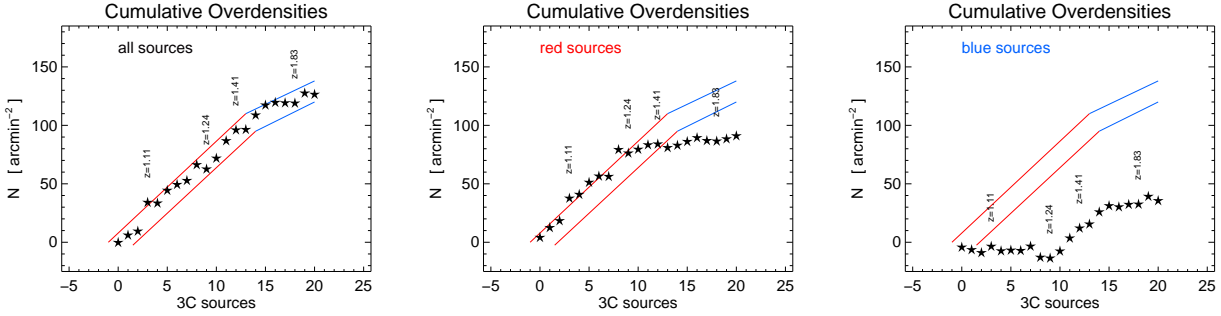


Fig. 10 Cumulative overdensities using method 1. Left: all candidates, middle: red candidates, right: blue candidates. The overdensities are the central surface densities after subtraction of the outer annulus ($> 55''$). The X-axis refers to the index of the 3C sources sorted by redshift. The two blue and red parallel lines embrace the range of ODs in the left panel with a gradient change around $z \approx 1.4$; for comparison the parallel lines are also shown in the middle and right panels.

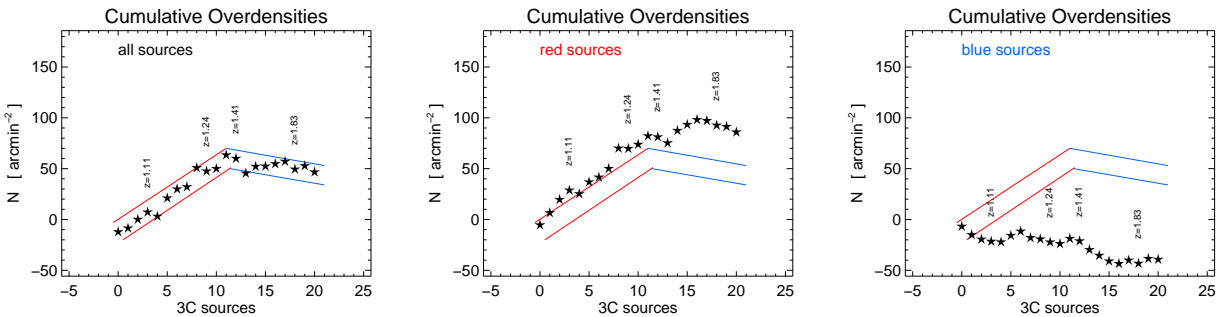


Fig. 11 Cumulative overdensities as in Fig. 10, but for a different candidate selection, method 2 ($22 \text{ mag} < F140W < 24 \text{ mag}$) as explained in Section 7.

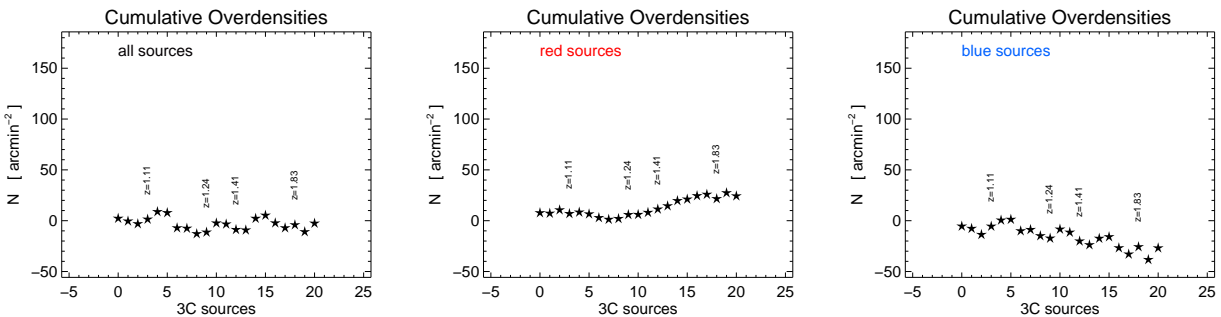


Fig. 12 Cumulative overdensities as in Fig. 11, but for very faint sources ($F140W > 24 \text{ mag}$) as explained in Section 7 and Appendix B.

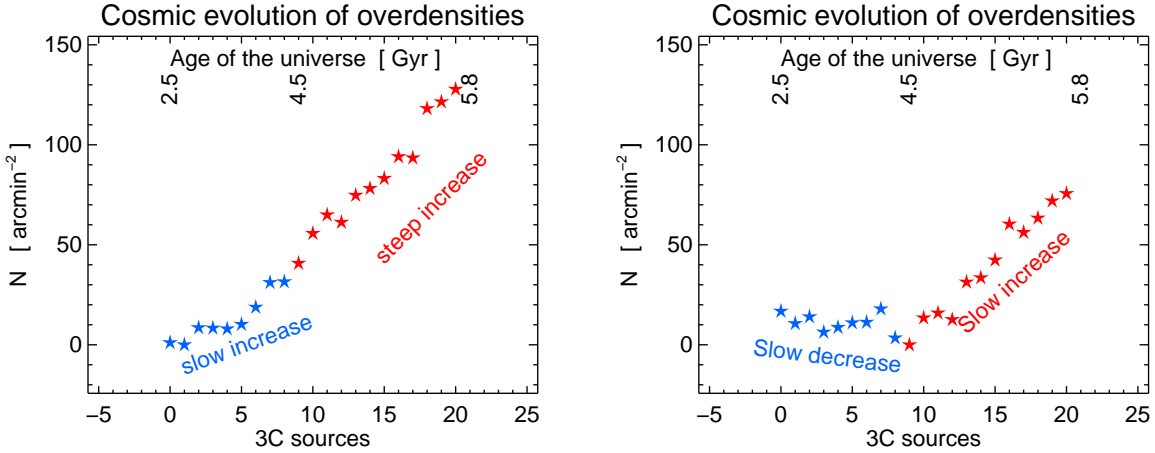


Fig. 13 Evolution of central overdensities versus age of the universe. **Left:** Using method 1 to select candidate cluster member galaxies at the 3C's redshift via SED fitting with local red and blue galaxy templates. **Right:** Using method 2 selecting candidate cluster member galaxies via $22 \text{ mag} < F140W < 24 \text{ mag}$.

observed such large images at Magellan and Lowell, reaching $r = 26$ mag, which should be sufficiently deep to detect all blue candidates.

The overdensity decline of the red galaxies starts at different redshifts for the two selection methods: $z \sim 1.24$ for method 1 and $z \sim 1.8$ for method 2. The two selection methods used different color ranges $F606W - F140W$ to define red sources: a redshift independent range $F606W - F140W > 2.0$ for method 2, while method 1 used a redshift dependent range which becomes redder with increasing redshift (roughly $F606W - F140W \sim 3 - 4$ at $z = 1$ and $F606W - F140W \sim 4 - 5$ at $z = 2$). Because at high redshift the galaxies are in a younger evolutionary state and might be bluer, method 1 is biased against red sources. (An exception may be dust enshrouded starburst galaxies.) Therefore the results from method 2 should be preferred. The lack of overdensities of red galaxies at high redshift ($z > 1.8$) needs to be investigated further by deeper data (see Appendix B).

We have also performed the candidate selection method 2 for the very faint sources ($F140W > 24$). Figure 12 shows the cumulative OD results. Considering all very faint sources shows, on average, no ODs. For the red sources there may be a small increase between $z \sim 1.2$ and $z \sim 1.8$. However, this should be considered with care because of the small number of red sources seen in the CMDs, as described in the Appendix B. The blue sources indicate a small OD decline, i.e. a central underdensity. This fits the scenario shown in Fig. 5 of West (1994) and further discussed in Appendix B.

8 Summary and outlook

Figure 13 summarises the evolution of the central overdensities found by the two selection methods of candidate cluster member galaxies at the 3C's redshift.

Acknowledgement: This research has made use of the

NASA/IPAC Extragalactic Database (NED) and of the NASA/ IPAC Infrared Science Archive, which is operated by the Jet Propulsion Laboratory, California Institute of Technology, under contract with the National Aeronautics and Space Administration. This work is based in part on observations made with the *Spitzer Space Telescope*, which was operated by the Jet Propulsion Laboratory (JPL), Caltech under a contract with NASA. Some of the data presented in this paper were obtained from the Mikulski Archive for Space Telescopes (MAST). STScI is operated by the Association of Universities for Research in Astronomy, Inc., under NASA contract NAS5-26555. Support for MAST for non-*HST* data is provided by the NASA Office of Space Science via grant NNX09AF08G and by other grants and contracts.

References

- Best, P. N. 2000, MNRAS, 317, 720
- Best, P. N., Lehnert, M. D., Miley, G. K., & Röttgering, H. J. A. 2003, MNRAS, 343, 1
- Galametz, A., Stern, D., De Breuck, C., et al. 2012, ApJ, 749, 169
- Ghaffari, Z., Westhues, C., Haas, M., et al. 2017, Astronomische Nachrichten, 338, 823
- Haas, M., Willner, S. P., Heymann, F., et al. 2008, ApJ, 688, 122
- Hilbert, B., Chiaberge, M., Kotyla, J. P., et al. 2016, ApJS, 225, 12
- Kotulla, R., Fritze, U., Weilbacher, P., & Anders, P. 2009, MNRAS, 396, 462
- Kotyla, J. P., Chiaberge, M., Baum, S., et al. 2016, ApJ, 826, 46
- Miley, G. & De Breuck, C. 2008, A&A Rev., 15, 67
- Peng, C. Y., Ho, L. C., Impey, C. D., & Rix, H.-W. 2010, AJ, 139, 2097
- Schlafly, E. F. & Finkbeiner, D. P. 2011, ApJ, 737, 103

- Seymour, N., Stern, D., De Breuck, C., et al. 2007, ApJS, 171, 353
- Spergel, D. N., Bean, R., Doré, O., et al. 2007, ApJS, 170, 377
- Spinrad, H., Marr, J., Aguilar, L., & Djorgovski, S. 1985, PASP, 97, 932
- Venemans, B. P., Röttgering, H. J. A., Miley, G. K., et al. 2007, A&A, 461, 823
- West, M. J. 1994, MNRAS, 268, 79
- Wylezalek, D., Galametz, A., Stern, D., et al. 2013, ApJ, 769, 79

9 APPENDIX A: Color magnitude diagrams

10 APPENDIX B: Very Faint Candidates

The CMDs (Figs. 14 - 20) show a paucity of sources which are very faint ($m_{F140} > 24$) and red ($F606W - F140W > 2.0$). These sources either do not exist or they escaped detection. They would have $F606W > 26$ mag. In principle, $F606W$ sources should be detected down to $F606W = 28$ mag, as indicated by the log(N) vs. mag diagram shown in Fig. 2. If true, then the majority of very faint and red sources should have been detected up to $F606W - F140W = 4.0$.

We checked visually the *HST* maps to look for such sources which are very faint and red, i.e. which are detected in $F140W$ but not in $F606W$.

We find that, in addition and compared to the cataloged very faint sources, there are about 20% more very faint sources in $F140W$. About half of them are detected in $F606W$ and half are not, suggesting that half are red and half are blue ($F606W - F140W < 2.0$). Furthermore, they appear to be rather homogeneously distributed across the images and not to be concentrated around the 3C sources. This would be consistent with the scenario, as shown in Figure 5 of West (1994). There, at the begin of the cluster assembly many faint galaxies are distributed farther away from the cluster center. During the cluster evolution, they will “travel” towards the cluster center and merge with each other and the resulting brighter galaxies are preferentially found at the cluster center. Nevertheless, this has to be checked further, perhaps with large deep optical images.

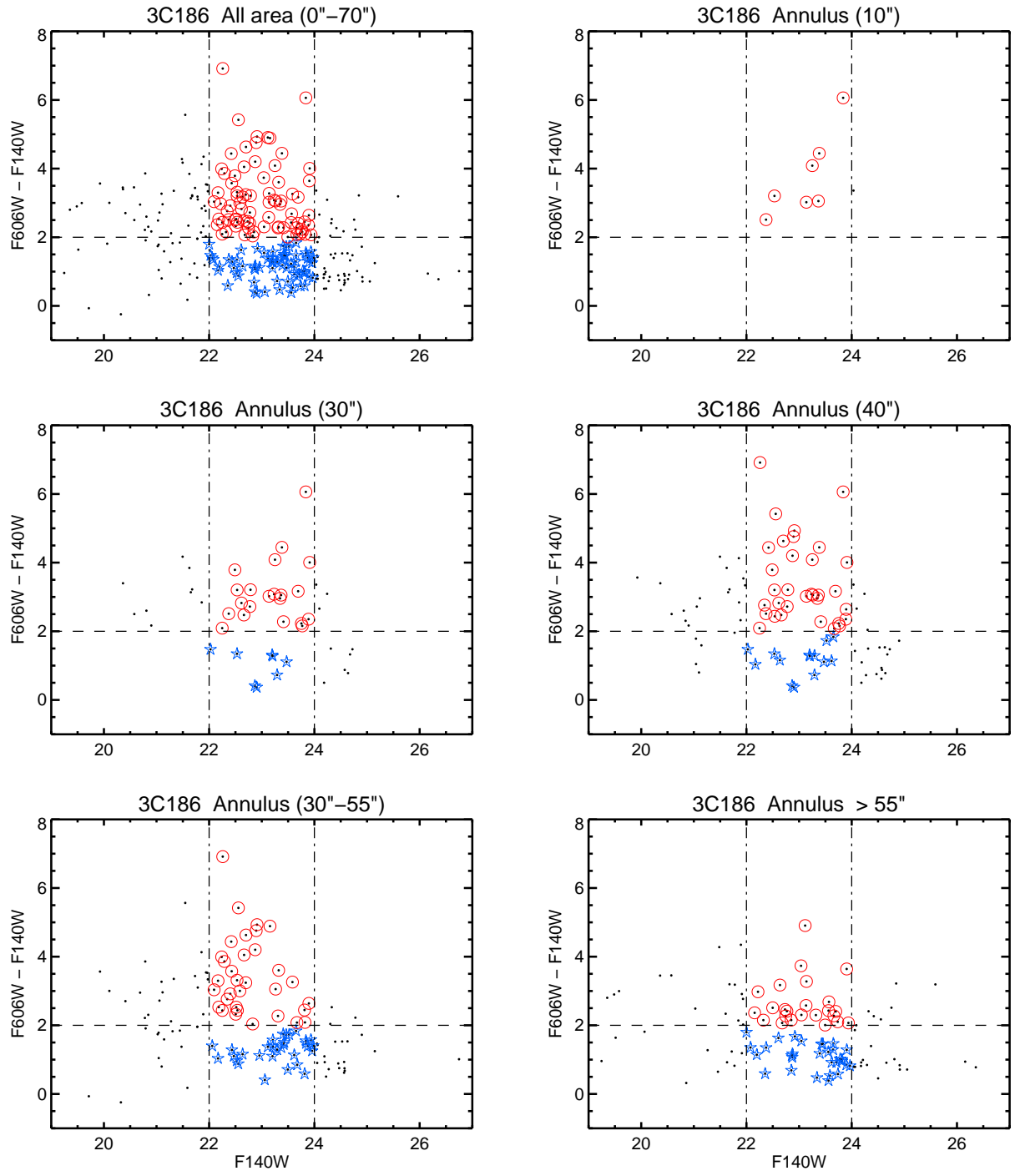


Fig. 14 CMDs of 3C 186. For explanations see Section 7.

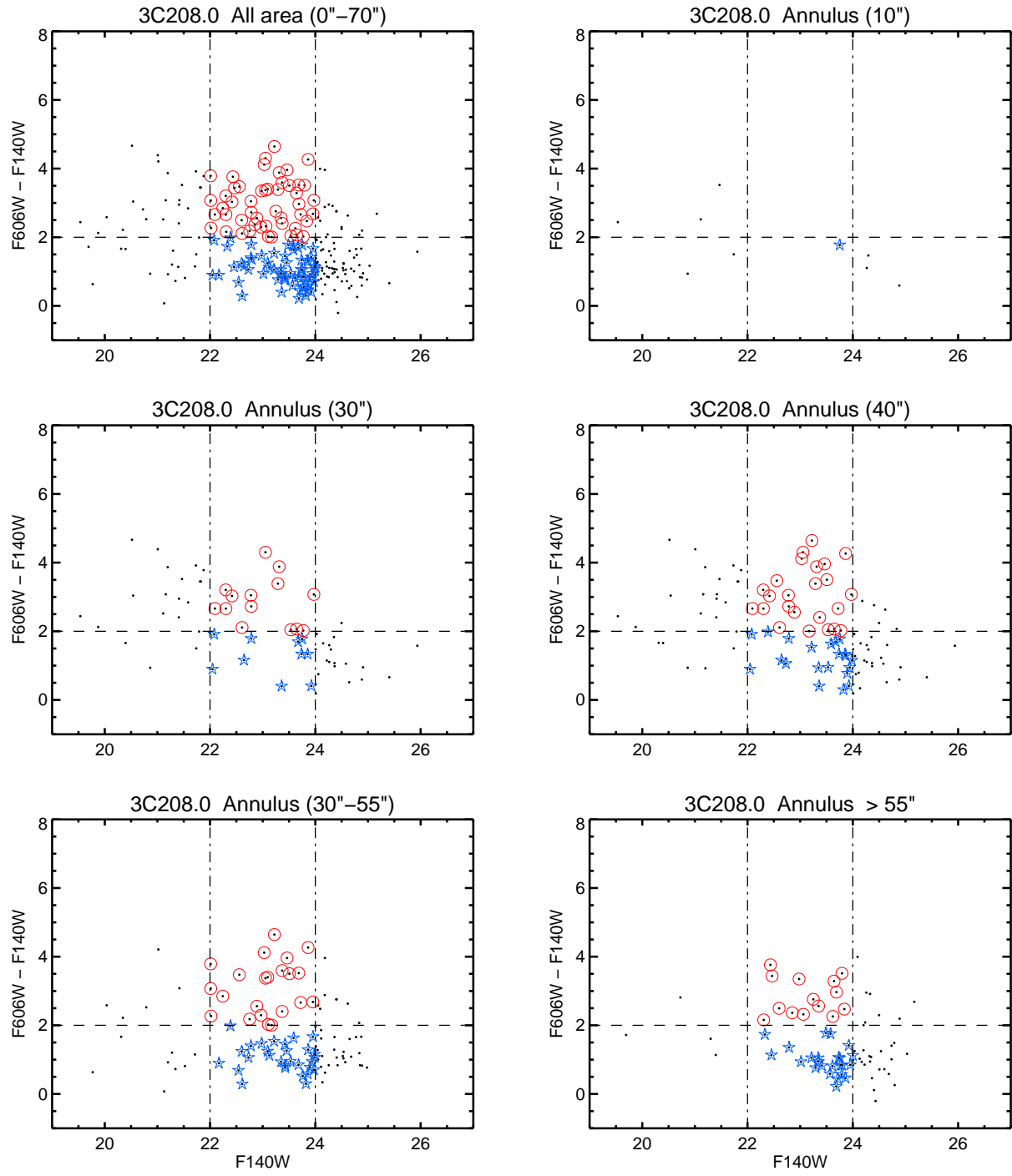


Fig. 15 CMDs of 3C 208.0. For explanations see Section 7.

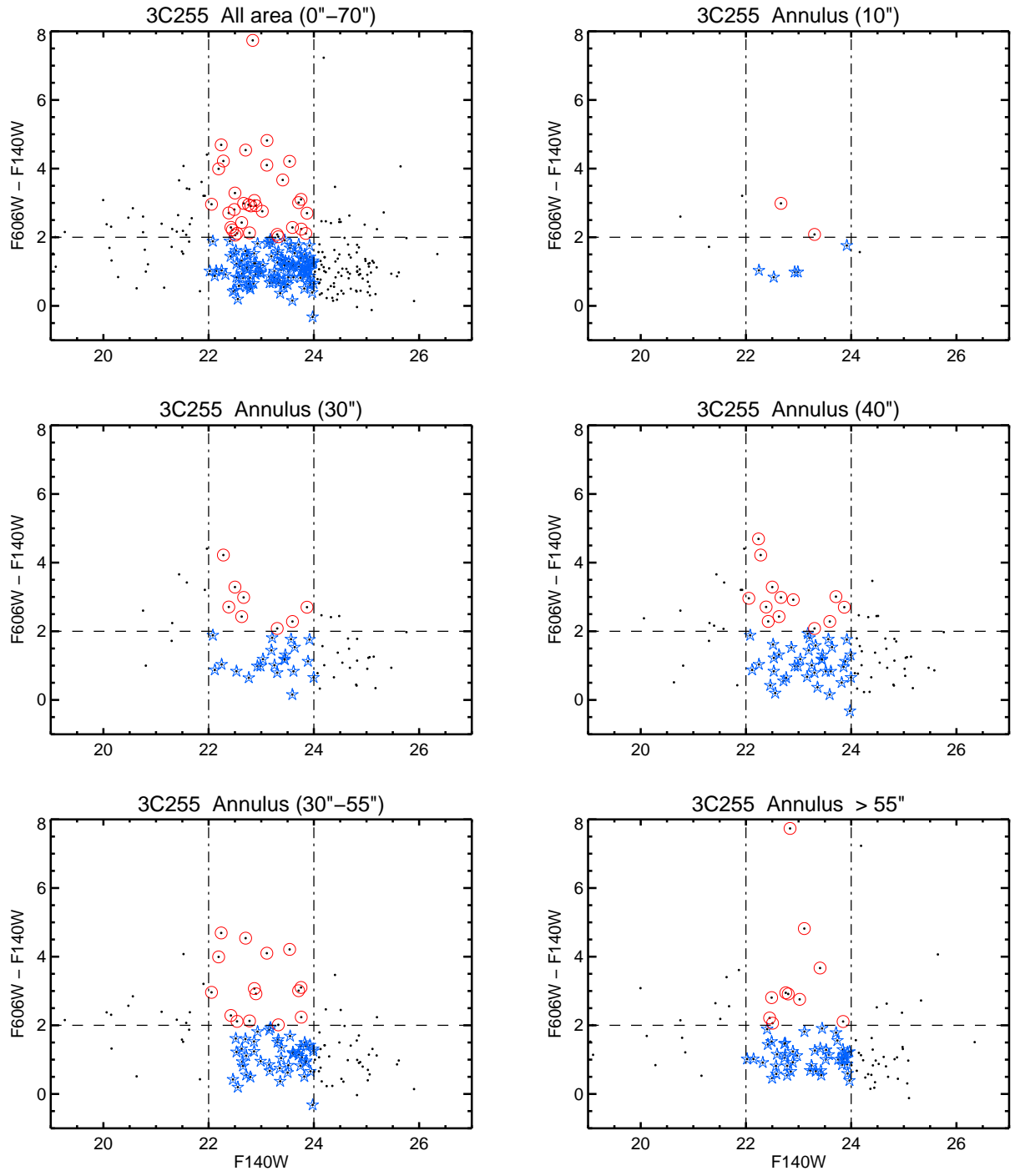


Fig. 16 CMDs of 3C 255. For explanations see Section 7.

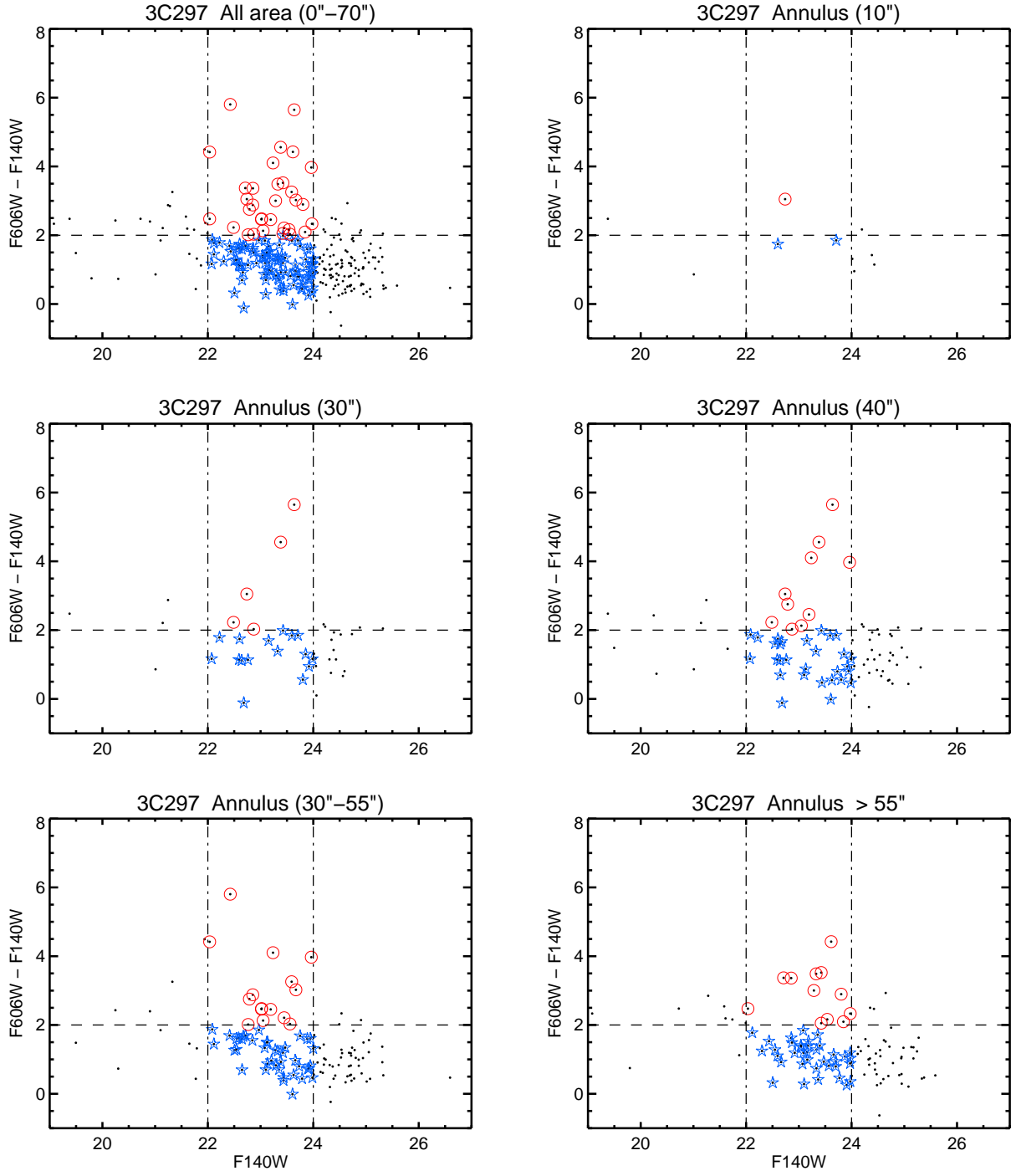


Fig. 17 CMDs of 3C 297. For explanations see Section 7.

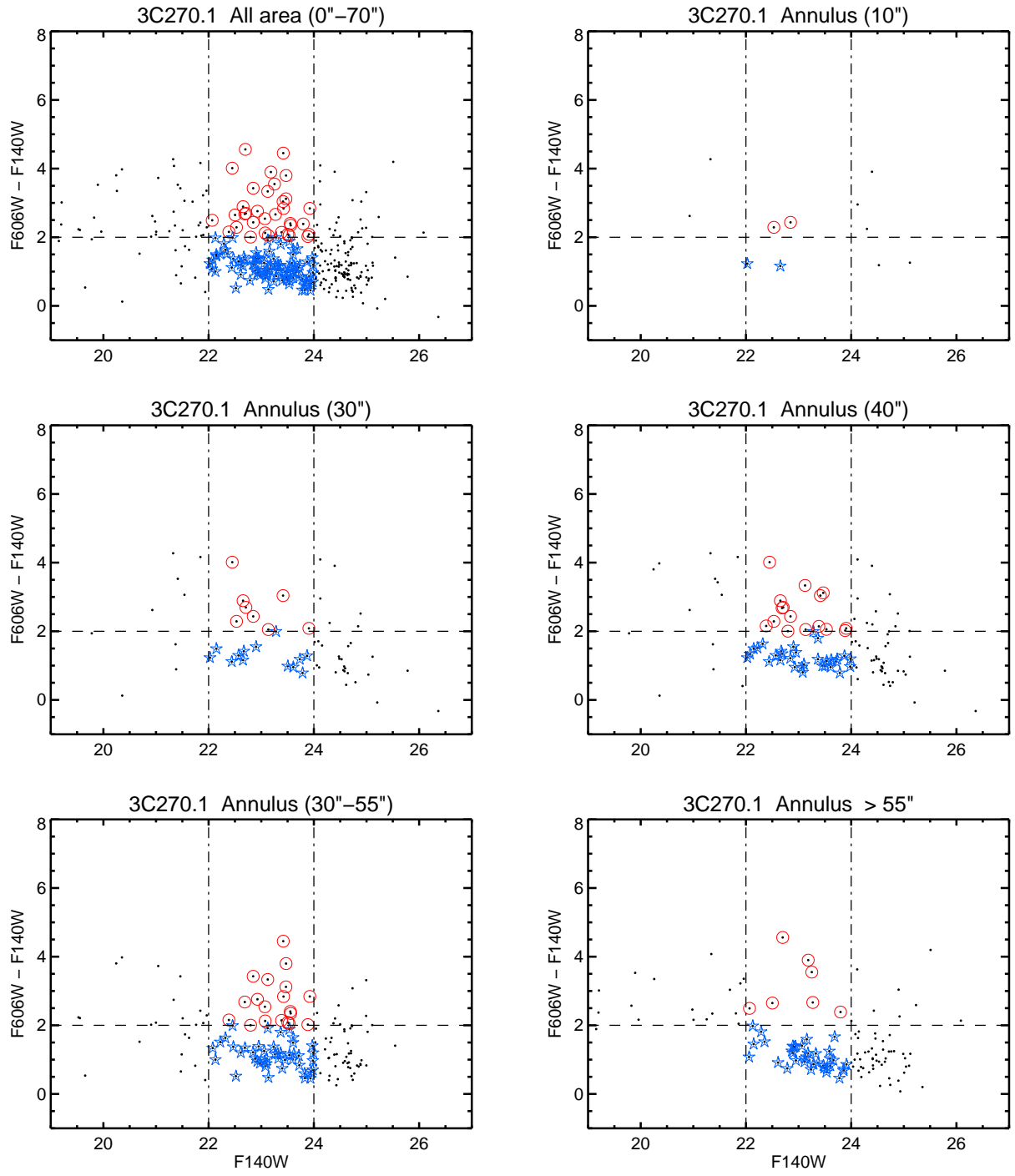


Fig. 18 CMDs of 3C 270.1. For explanations see Section 7.

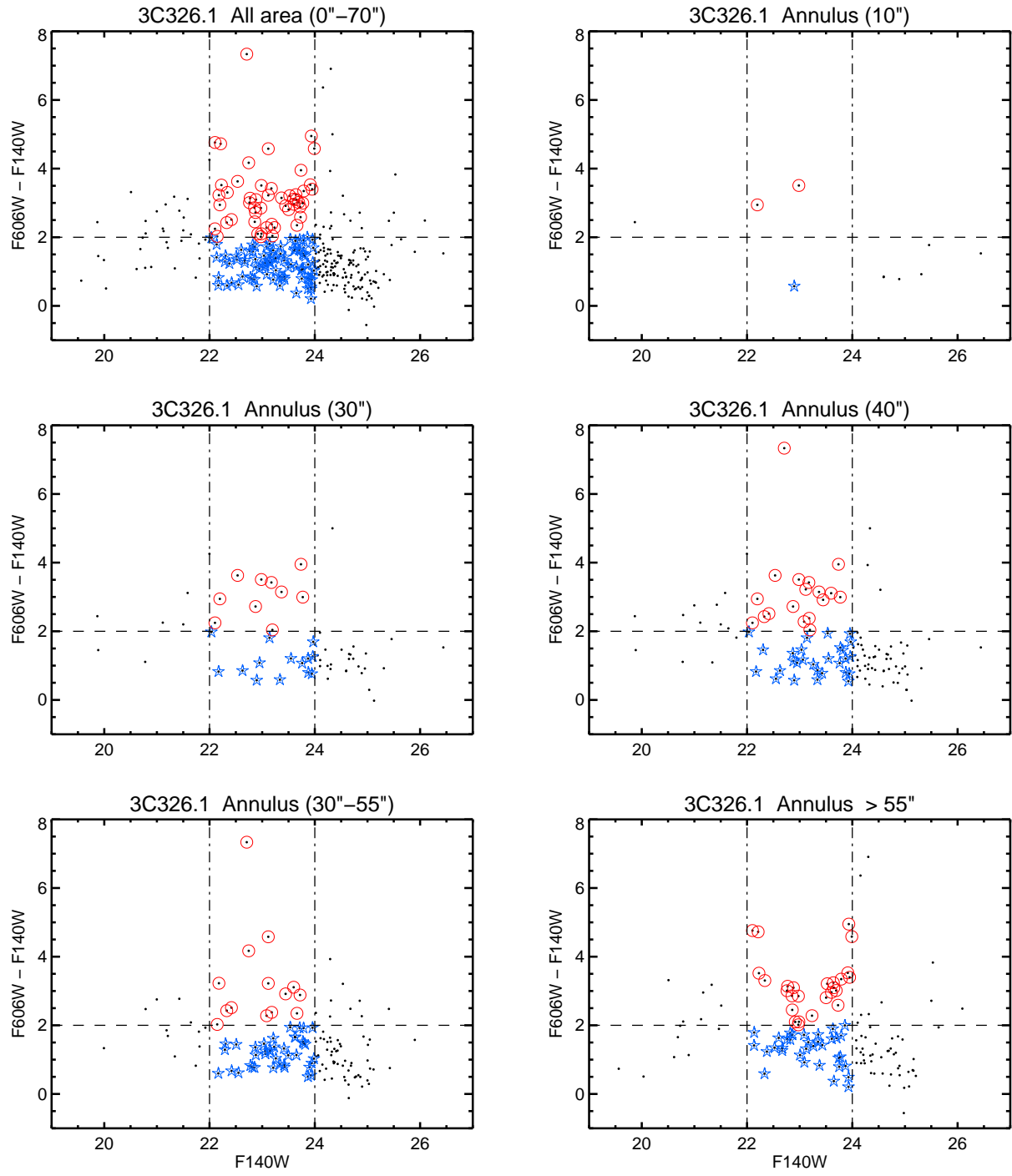


Fig. 19 CMDs of 3C 326.1. For explanations see Section 7.

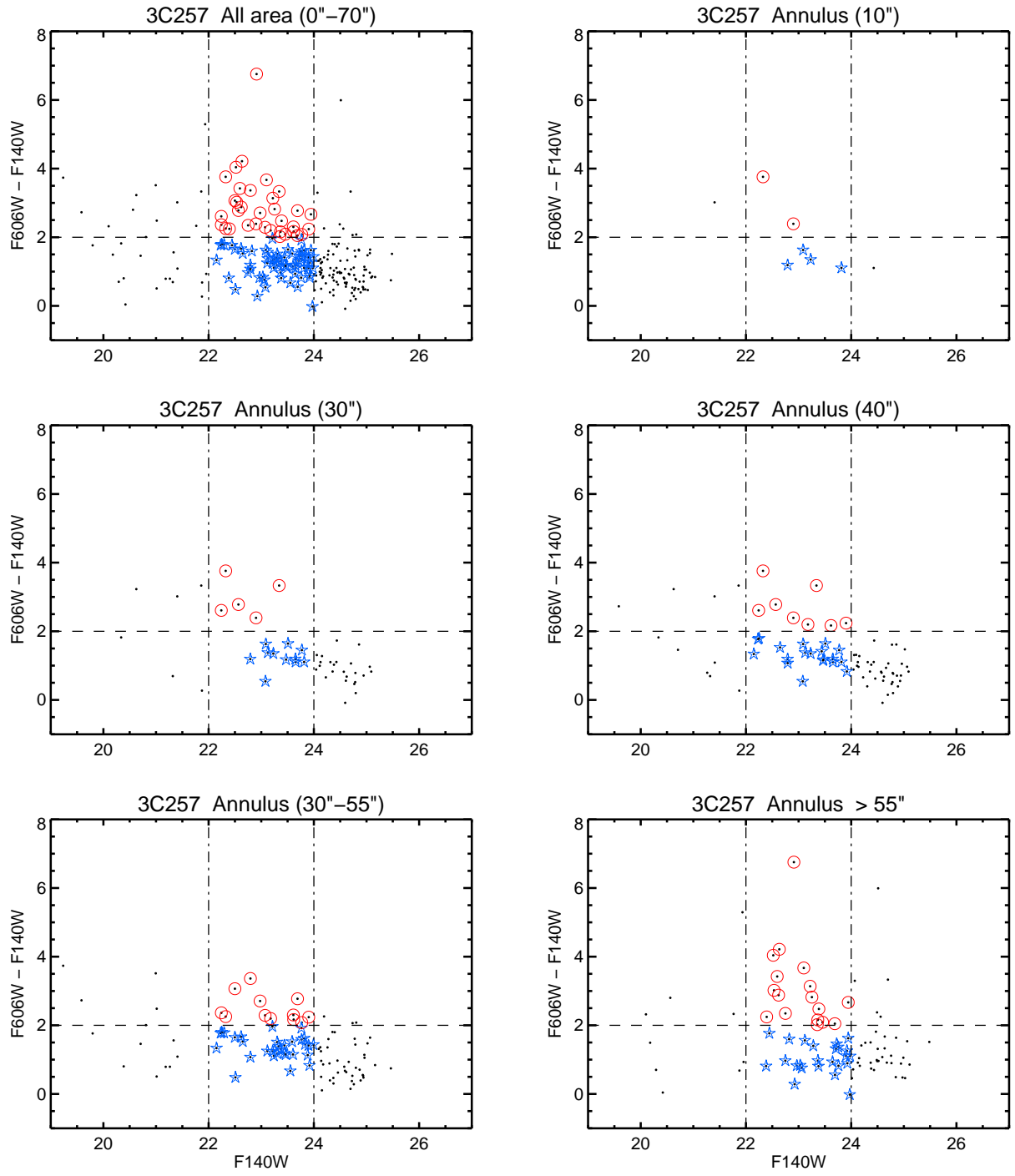


Fig. 20 CMDs of 3C 257. For explanations see Section 7.

1 Name	2 redshift	3 Type	4 n_{all}	5 n_{red}	6 n_{blue} $30''$	7 n_{all}	8 n_{red} $30 - 55''$	9 n_{blue}	10 n_{all}	11 n_{red} $> 55''$	12 n_{blue}	13 $n_{red\ ours}$ $40''$	14 $n_{ETG\ Kotyla}$ $40''$
3C 068.1	1.238	QSO	15	2	13	30	14	16	37	9	28	10	9
3C 186	1.069	QSO	18	10	8	49	21	28	27	7	20	15	8
3C 208.0	1.112	QSO	30	18	12	37	24	13	22	6	16	25	15
3C 210	1.169	RG	29	20	9	41	11	30	38	4	34	23	17
3C 220.2	1.157	QSO	17	9	8	43	8	35	27	10	17	11	10
3C 230	1.487	RG	16	3	13	31	7	24	13	3	10	7	6
3C 255	1.355	RG	15	4	11	27	5	22	16	3	13	6	6
3C 257	2.474	RG	4	3	1	4	0	4	10	2	8	3	8
3C 268.4	1.402	QSO	19	3	16	27	3	24	15	0	15	4	11
3C 270.1	1.528	QSO	13	4	9	35	6	29	13	3	10	7	12
3C 287	1.055	QSO	23	8	15	55	10	45	48	10	38	9	7
3C 297	1.406	RG	15	2	13	26	4	22	16	3	13	4	12
3C 298	1.438	QSO	9	0	9	16	2	14	18	5	13	0	4
3C 300.1	1.159	RG	23	8	15	38	14	24	42	17	25	15	7
3C 305.1	1.132	RG	15	5	10	45	2	43	32	5	27	7	5
3C 322	1.168	RG	10	4	6	19	11	8	17	3	14	8	4
3C 324	1.206	RG	25	11	14	37	9	28	34	6	28	16	15
3C 326.1	1.825	RG	9	4	5	14	4	10	19	9	10	5	14
3C 356	1.079	RG	22	9	13	40	8	32	40	9	31	11	12
3C 432	1.785	QSO	6	0	6	12	3	9	13	4	9	2	12
3C 454.1	1.841	RG	14	2	12	23	3	20	15	1	14	3	9

Table 1 Sample and overdensity results using method 1. In the two last columns 13, 14 we compare our results on the red candidates within $40''$ with the number of Early Type Galaxies found by Kotyla et al. (2016).